British Journal of Applied Science & Technology
15(5): 1-19, 2016, Article no.BJAST.25264
ISSN: 2231-0843, NLM ID: 101664541

SCIENCEDOMAIN *international*
www.sciencedomain.org

Experimental Investigation of Shear Behavior of Deep RC T-beams Under Indirect Loading

Yousif Jabbar Lafta[1,2*] and Kun Ye[1]

[1]School of Civil Engineering and Mechanics, Huazhong University of Science and Technology, Wuhan, China.
[2]Department of Civil Engineering, University of Basra, Basra, Iraq.

Authors' contributions

This work was carried out in collaboration between both authors. Author YJL designed the study, performed the statistical analysis, wrote the protocol, wrote the first draft of the manuscript and managed literature searches. Author KY managed the analyses of the study and literature searches. Both authors read and approved the final manuscript.

Article Information

DOI: 10.9734/BJAST/2016/25264
Editor(s):
(1) Manoj Gupta, Department of Mechanical Engineering, NUS, 9 Engineering Drive 1, Singapore 117576, Singapore.
(2) Elena Lanchares Sancho, Department of Mechanical Engineering, University of Zaragoza, Zaragoza, Spain.
Reviewers:
(1) Alcinia Zita Sampaio, Technical University of Lisbon, Portugal.
(2) Ahmed Abdelraheem Farghaly, Sohag University, Egypt.
Complete Peer review History: http://sciencedomain.org/review-history/14277

Original Research Article

Received 25th February 2016
Accepted 4th April 2016
Published 21st April 2016

ABSTRACT

The main goal of present study is to experimentally and analytically investigate the behavior of indirect loading, deep flanged reinforced concrete (RC) beams. The load is applied via shear on the side arms of the beam with bearing plates. Eighteen reinforced concrete deep T- beams designed to fail in shear. The beams without web reinforcement were tested under indirectly loading conditions. The beams were divided into three groups according to the ratio of shear span to effective depth. The specimens had different flange depth and flange width in order to investigate the effects of flange dimensions. The behavior of beams was observed; cracking load, ultimate loads, concrete strain, deflections and crack widths. Experimental results indicate that the indirectly loaded deep beams can carry additional loads after diagonal cracking.
The study includes numerically predicted the Ultimate Loads carrying capacity with strut-and-tie method (STM) which is based on the ACI Building Code (318-08). The prediction results of ultimate shear capacity for (STM) models are agreed with the experimental finding. As well as the

**Corresponding author: E-mail: y.jabbar@yahoo.com;*

performance of the beams conformed with 3D non-linear finite element analysis that involves discrete reinforcement modeling. This modeling process is performed by using ANSYS 12.1 the prediction results of ultimate shear capacity for Ansys models are agreeing with the experimental finding. Furthermore, the experimental results were compared with prediction data used the equation for ordinary beams that recommended by ACI Building Code (318-08). It was concluded that the ACI Code equation underestimated the concrete shear strength of the single span indirectly loaded Flanged deep beams.

Keywords: Deep T-beam; flange depth; flange width; shear span to effective depth; strut-and-tie, indirect load.

1. INTRODUCTION

Nowadays, many building codes concerned with Shear design provisions distinguish between regions in normal size beams, relating to the shear span to effective depth ratio.

Regions in beams with short spans are categorized as D-regions where the D refers to disturbed or deep when the portion of a member have a distance equal to the member height or effective depth from a force discontinuity or a geometric discontinuity as defined by ACI building Code 318R-08 [1]; in which the load is transferred by the arch action mechanism and the distribution of strain is nonlinear across the section of the beam. And B-region where the B refers to beam or Bernoulli, in which the load is carrying by beam action and distribution of strain is linear across the section as well as ACI building Code 318R-8 defined deep beams as the members loaded on one face and supported on the opposite face so that compression struts can develop between the loads and the supports, and have either with clear span equal to or less than four times the overall member depth, or regions of beams loaded with concentrated loads within twice the member depth. And it is recommended taking into account the nonlinearity of strain distribution and lateral buckling in the design of deep beams. Also in the longer shear spans, the Regions in reinforced concrete beams where the shear span is less than 2h defined as D-region. Park [2] defined the beam which has a shear span to depth ratio less than 2 of simply supported beams, or less than 2.5 for any span of a continuous beams, as deep beam.

The behavior of deep beams is different from that of common flexural members; the behavior of deep beams is governed by shear rather than flexure since a large portion of compressive force is directly transferred to supports, and the shear strength is much greater than that of ordinary beams. Deep or short beam grow inclined cracks showed by Syroka [3] and tan [4], capable to carry further load by compressive strut through arch action.

In many instances reinforced concrete slabs together with the beams behaves T-sections. the Stronger compression zones provided with flanges in T-sections observed by Kalyanariman et al. [5] and Kong [6] generally precludes shear, compression failure in T-beams and as a result improves the shear strength capacity. The shear strength of flanged deep beams is a function of many factors such as concrete compressive strength, main and web reinforcement, slenderness (shear span/effective depth ratio), loading and supporting conditions, flange size and beam depth. According to the Fereig and Smith [7], Heywood [8], Simply supported deep beams may be classified according to loading and supporting conditions as directly loaded (forces applied on the top and reactions on the underside), and indirectly loaded beams (loads applied to the sides of members) as in the headstocks supporting beams on nibs' side face. Fig. 1 shows the direct and indirect loaded.

The tested short shear span beams by Ferguson [9], Taylor [10], and Neville and Taub [11] deals with indirectly loaded (shear span-to effective depth ratios of 1.35, 1.64, and 2.09) conclude that the large portion of the additional strength associated with small shear span-to-effective depth ratios had been lost. While Kalyanariman et al. [5] observed that the tensile stress in steel was distributed nonuniformly over the length before diagonal tension cracks were formed in single span deep beams with flanges were indirectly loaded via side arms where the shear span to depth ratio of tested specimens were 1.0 and 1.35. In addition, the tensile stress gradually became uniform over the length of steel bars after diagonal tension cracks were formed attributed to the tied arch action commonly encountered in deep beams.

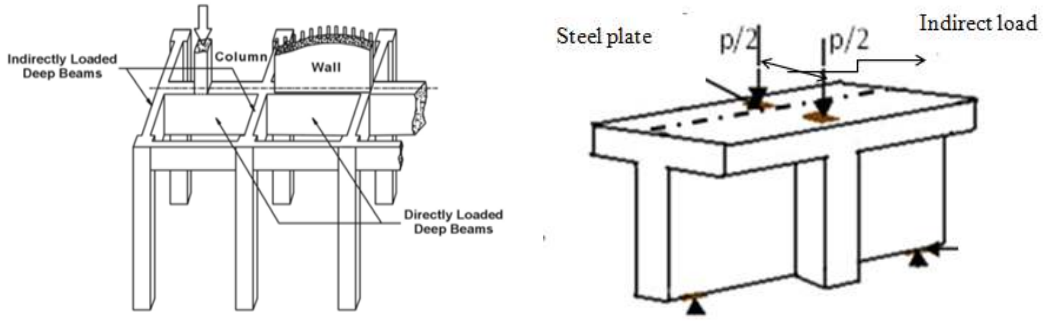

Fig. 1. Directly or indirectly loaded deep beam

Test results showed that indirectly loaded deep T-beams could have as much as 70% higher shear strength than that of indirectly loaded deep rectangular beams related to the influences of the loading and supporting conditions observed by Zsutty [12]. However, investigation of the performance of indirectly loaded reinforced concrete deep beams is quite lacking and needs further researches concerned with the performance of reinforced concrete deep beams with flanges subjected to indirectly loading. As well as no data have been reported on flanges size effects on shear capacity, deformation and failure manner of indirect loaded deep beams.

The main object of this paper is to investigate the structural behavior of indirectly loaded single span RC deep beams with flanges to evaluate the influence of flange dimensions on structural behavior of the beams. The study consists of an experimental work in which eighteen reinforced concrete deep T-beams were tested with different flange size and different shear span to effective depth ratio (a/d). All beams were reinforced with the same amount and arrangement of tensile steel, without shear reinforcement and the shear span to effective depth ratio (a/d) was varied as (1.0, 1.4, and 1.8). During the testing period, ultimate loads, crack width, deflection, and strains are recorded. Tied arch will be formed after the appearance of diagonal cracking. An important part of applied load is transmitted directly from point of applied load to support by a diagonal compressive strut. While the horizontal compression stress in concrete and the tensile stress in the main reinforcement have to equilibrate the load. The geometry of this technique is clearly depends on location of loads and reactions.

The Failure phenomenon commonly due to splitting in diagonal compressive strut that related to a splitting test of concrete cylinder. Figs. (6, 7 and 8) show the crack pattern of the beams. Strut-and-tie method is one of the most simple and applicable methods which is used to simplify analysis and design of deep beams. The experimental results of ultimate shear strength are agreeing with predicted results using (STM). As well as 3D non-linear FE software package ANSYS used to model a typical RC deep T-beam under indirect loading as well as to predict and validate the experimental test result obtained by the authors, the test result good agreements with the predicted data by Ansys software. Relative to the equation for ordinary beams, ACI Code 318-8 underestimates the contribution of concrete shear strength of the flanged single span deep beams. Summarized, the experimental results showed the evident flange size effect on the shear strength of RC indirectly loaded deep T-beams.

2. EXPERIMENTAL INVESTIGATION

The tested beams having the span to depth ratio of 1, 1.4 and 1.8 were designated as group 1 (GRgroup 2 (GR2) and group 3 (GR3) respectively and each group consisted of six beams.

2.1 Casting of Beams

Wood forms were used in the fabrication of the beams. The inside of the forms was lubricated before the reinforcement cage was placed in position, the concrete mix was placed in three approximately equal layers and each layer compacted by means of poker vibrator, the top surface of the beam was finished level. The beams were moist cured by water for seven days under damp canvas and then stored in the laboratory to testing. 18 simply supported single span concrete deep beams divided into three

series are casting. Each group consists of six Specimens. All beams of T-cross section with web thickness b_w of (120 mm) and flange width b_f of (240 mm, 300 mm and 360 mm) and flange depth h_f of (60 mm and 90 mm).

The specimens have rectangular central transverse intersecting member with the same overall depth of the beams, (120 mm) width and length equal the flange width of the beams. Beams are tested to failure under indirectly point loads. The details and dimensions of the beams are given in Fig. 2.

All beams are single span and without shear reinforcement. The beams were designed to fail in shear, to satisfy this type of failure a suitable reinforcement was provided [13]. The design compressive strength was obtained in accordance with ASTM-C-39 [14] on cylindrical specimens with dimensions of 300 mm (height)×150 mm (diameter). The value of f_c` is obtained from the mean values of three concrete cylinders cured under the same conditions and tested on the same day as the specimens. After curing of 28 days all cylindrical specimens were tested. The measured compressive strength of the employed concrete is 25MPa and slump of about 120 mm. Two types of reinforcement are used in the specimens, namely, deformed steel for longitudinal reinforcement and smooth round steel for flange reinforcement and stirrups. The main beam is reinforced with 12 mm diameter deformed steel bars with yield strength of 330 Mpa and anchored behind the support with sufficient length [3] and with 90 degree bent in order to prevent the anchorage zone failure.

The intersecting beam is reinforced with 16 mm diameter deformed steel bars with yield strength of 330 MPa. Stirrups of 6mm diameter with yield strength of 450 MPa. These are average values achieved from 3 bars of 600 mm length for each type of steel bar. Bearing plates of (120 mm width, 10 mm thickness and 100 mm length) were seated at loading and supporting points in order to avoid concrete local crushing failure as shown in Fig. 5. The specimen notation is typically written as `TB1Gr1', where TB1 is the number of beams in the series of (TB1, TB2, …., TB6); and character (Gr1, Gr2, and Gr3) was definitely the three beam's series of different a/d ratios.

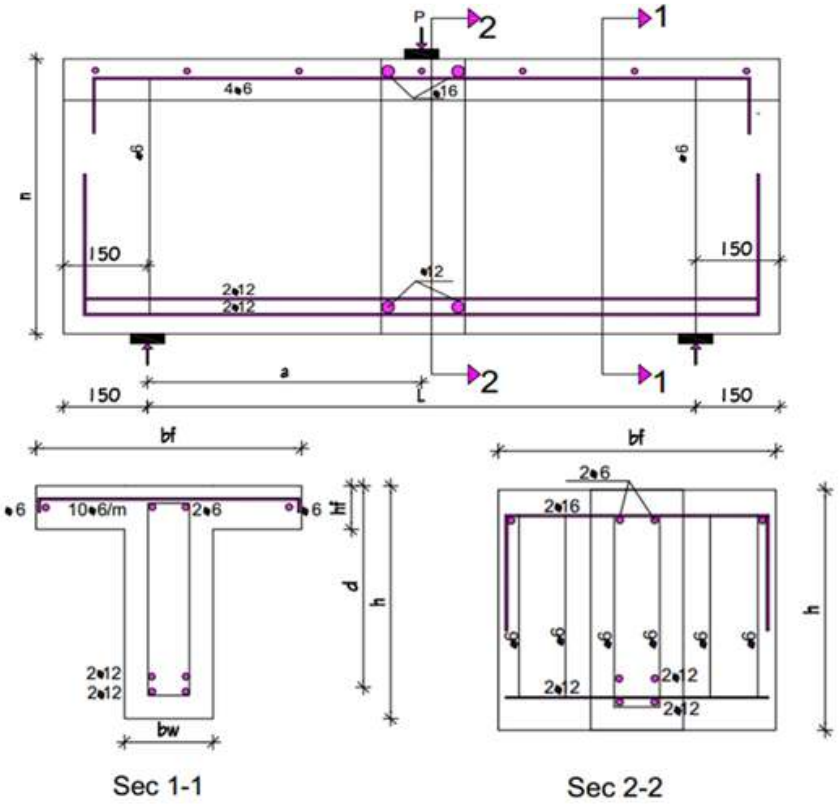

Fig. 2. Details of tested beams and sections

2.2 Testing of Beams

Two days before testing, the beams were painted to facilitate tracing the cracks. Aluminum discs with a 10 mm diameter and central hole of 1.5 mm diameter are used to measure the surface strain. The positions of the discs, points are marked and the discs are attached using an epoxy resin as shown in Fig. 3.

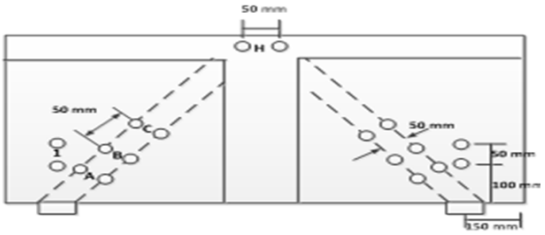

Fig. 3. Demic disc arrangement in tested beams

Typical arrangement and experimental setups are shown in Figs. 4 and 5.

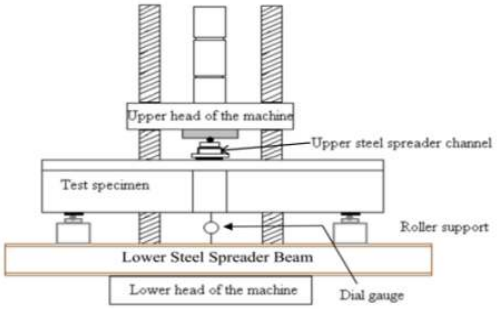

Fig. 4. Test setup

A steel spreader beam is used to affect two equal point loads. It is seated on two pins support which placed on top of the beams. The support in beams' ends has two types; roller and pin. The bottom spreader consisted of two universal steel I-beams with a depth of 200 mm. Torsee's Universal Testing Machine (UTM) with capacity of 2000 kN was used to apply the load. Mid span deflections were measured by (0.01 mm) accuracy dial gauge (ELE type) and (30 mm) capacity placed underneath the center of the bottom face of specimens. A mechanical type Demec Gauge (Lc= 0.002 mm) was used to measure surface concrete strain at every stage of loading. The beams were loaded from the top via the intersecting member at the center of beams span. Load was applied incrementally. At each load increment, the total applied load on the beam, mid-span deflection, and crack width have been measured. The crack width is measured by using a hand microscope and plotted and marked. A test was terminated when the total load on the specimens started to drop off.

Fig. 5. Test arrangement

2.3 Experimental Results and Discussions

2.3.1 Behavior of beams under loading and crack pattern

All the tested beams failed in shear. No local failure due to crushing of concrete under the load or over the supports was observed. End anchorage of the main bars functioned properly during testing and did not affect the mode of beam failure. Crack patterns after failure are shown in Figs. 6, 7 and 8.

2.3.2 Behavior of group (1) a/d = 1.0

It was noticed that, the inclined cracks in the shear span of indirectly loaded T-beams occurred suddenly with a thud at mid depth along the line between the applied load and supports. As the load increased, the major inclined crack became wider and extended towards the load and supports then extended through the compression flange near the failure.

2.3.3 Behavior of group (2) a/d=1.4

Few fine flexural cracks was gradually noticed at the bottom of the beam near mid span, but they still with so small crack width in spite of increasing the load. By increasing the load the numbers of cracks increased and development of major diagonal cracks between the load and each support.

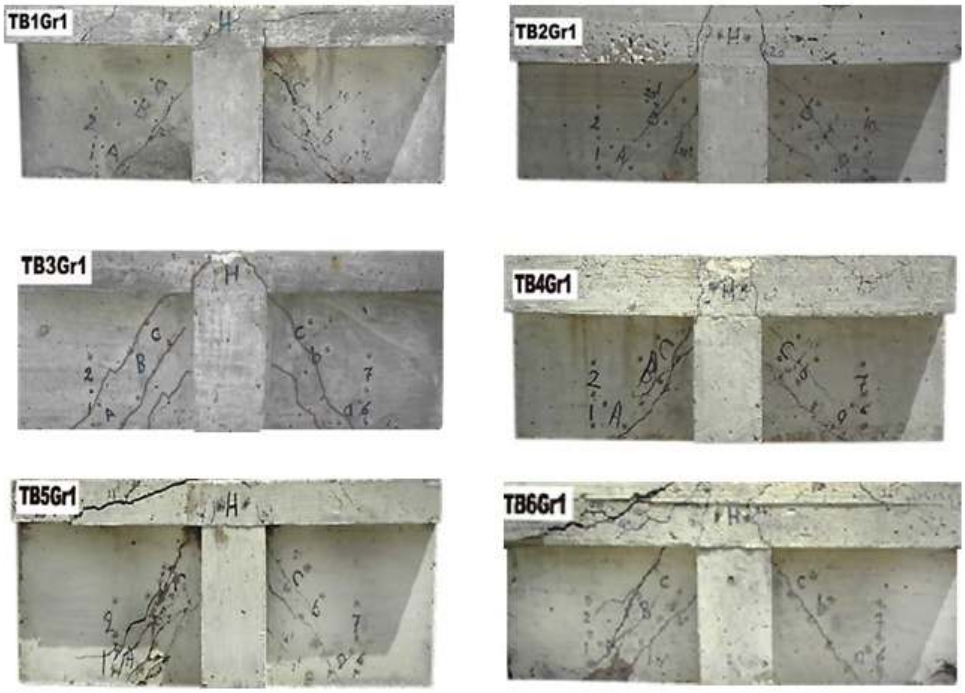

Fig. 6. Crack patterns for beams of group 1

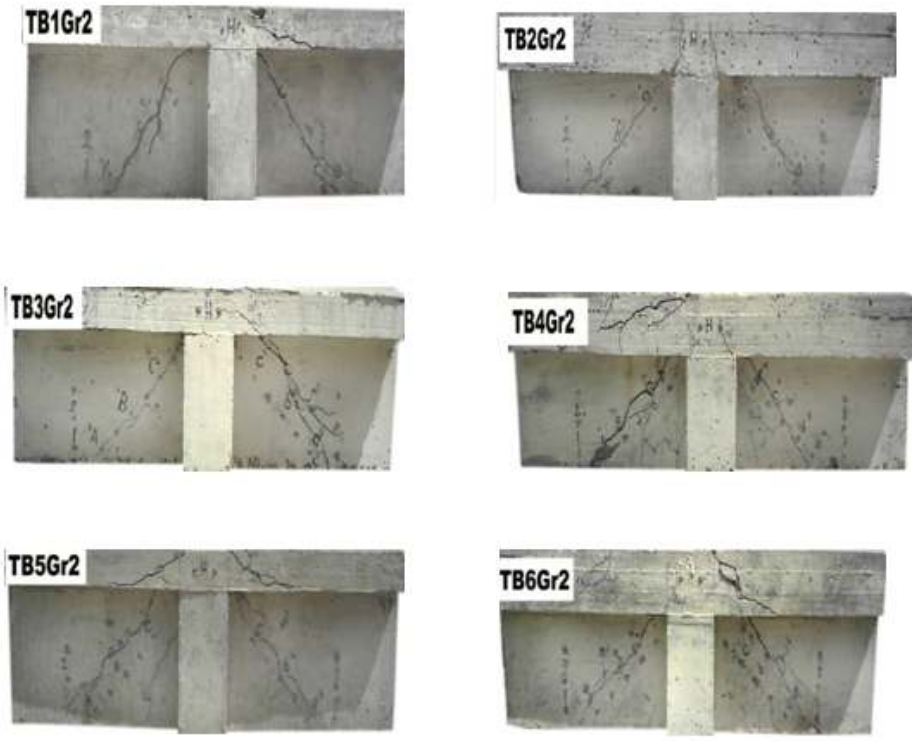

Fig. 7. Crack patterns for beams of group 2

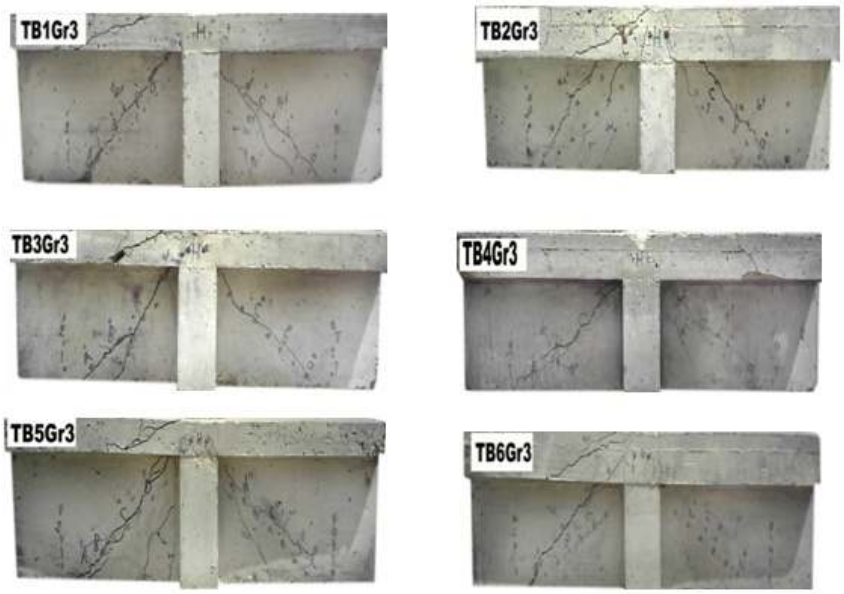

Fig. 8. Crack patterns for beams of group 3

2.3.4 Behavior of group (3) a/d=1.8

The behavior of this group was similar to previous groups, however the number of flexural cracks extend upwards with increasing load but still of less width, until shear failure by diagonal cracks. For all indirectly loaded T-beams were observed that more diagonal cracks appear before failure parallel to the strut line between load and support, but almost failure occurs by the major diagonal crack between load and support. For all groups, deflection at mid-span can be regarded as a measure of ductility, increased with increasing the a/d ratio.

2.3.5 Inclined cracking and ultimate load

Inclined cracking and ultimate load are listed in Table 1. Inclined cracking load is defined as the load at which the first major inclined crack appears in the shear span. The ratios of inclined cracking to ultimate load ranged from (0.36 to 0.67) with an average value of (0.52) and standard deviation of (0.08). The variation in a/d ratio seems to have a significant effect on the ultimate load. From Table 1 it can be shown from value of non-dimension (R) that the beams with the same flange width and 90 mm flange depth exhibited higher ultimate load than with 60 mm in the similar (a/d) ratio. Beams TB2,TB4, and TB6 of group (1) showed 37%, 38% and 10% higher ultimate loads than beams TB1, TB3 and TB5 of group (1); beams TB2, TB4 and TB6 of group (2) showed 10%, 15% and 26% higher ultimate loads than beams TB1, TB3 and TB5 of group (2); beams TB2 and TB4 of group (3) showed 11% and 10% higher ultimate loads than beams TB1 and TB3 of group (3). The up rise in ultimate loads of higher flange depth beams is attributed to the strong compression zone provided by increasing depth of the flanges. However the effect of flange width and flange depth on the ultimate loads is small as (a/d) ratio increase.

2.3.6 Effect of (a/d) ratio

The inclined cracking and the subsequent failure of reinforced concrete deep beams are strongly affected by the relative magnitudes of the shearing stress and flexural stress [15]. This effect may be conveniently considered as a function of (a/d) ratio. The distribution of stresses in the indirect loading beams after forming of inclined crack revealed a tendency towards the arch action, but not pure arch action since the force in the tension reinforcement was not constant through the span [7]. From Table 1 it is concluded that the increase of ultimate load is obtained by reducing (a/d) ratio. From comparisons of the ultimate load capacity of tested beams with different (a/d) ratio, it was noticed that, for beams with (60 mm) flange depth and (360 mm) flange width an increase of 67% is obtained by reducing (a/d) ratio of (1.8 to 1), for beams with (90 mm) flange depth and (360 mm) flange width an increase of 80% is

obtained by reducing (a/d) ratio of (1.8 to 1). Also the other beam shows the same behavior. This increase in ultimate load is attributed to the higher contribution of arch action shear transfer in beams with lower (a/d) ratio this confirms with Fereig and smith they conclude that The arch action is less for higher (a/d) ratio [7].

2.3.7 Deflection

Typical load-mid span deflection curves for beams in groups 1, 2, and 3 are shown in Figs 9, 10 and 11, respectively. It can be noticed that the formation of the first major inclined crack significantly reduced beams stiffness and tends largely to cause the change the slope of the curves. The amount of deflection is increased considerably with the span/effective depth ratio. The beams with 90 mm flange depth exhibits smaller deflection than beams with 60 mm flange depth with the same a/d ratio.

2.3.8 Effect of flange depth

It can be seen from Table 1 that the maximum loads are increased as the flange depth increased (with the same a/d ratio). This increase is attributed to the strong compressive zone provided by an increase in the flange depth. whereas, beams TB2Gr1, TB4Gr1, TB6Gr1 exhibit 34%, 3% and 9% higher first cracking load and 18%, 15% and 20% higher ultimate load compared with corresponding beams TB1Gr1, TB3Gr1 and TB5Gr1. In group 2 and group 3 the variation of the flange depth significantly affects the ultimate load but less for cracking loads. The load vs. mid-span deflection curves for beams of the same span and flange width show that mid-span deflection is increased as the flange depth is decreased as shown in Figs. 9, 10, and 11.

2.3.9 Effect of flange width

From Table 1 can be seen that the effect of flange width is small on ultimate load – carrying capacity f beams. Curves of mid-span deflection vs. span load showed that the increase of flange width leads to an increase in maximum deflection of beams with similar (a/d) ratio.

Table 1. Experimental inclined cracking and ultimate loads

Beam no.	Span load (kN)		P_{cr}/P_u	P_u/bhf'_c (R)	$\frac{P_U - P_{cr}}{P_{cr}} \times 100$
	Inclined cracking P_{cr}	Ultimate P_u			
a/d=1					
TB1Gr1	117.70	300.00	0.39	0.27	155%
TB2Gr1	156.96	353.00	0.44	0.37	125%
TB3Gr1	156.96	313.90	0.50	0.29	100%
TB4Gr1	160.96	360.00	0.45	0.40	124%
TB5Gr1	161.86	353.00	0.46	0.32	118%
TB6Gr1	176.95	372.78	0.47	0.35	111%
a/d=1.4					
TB1Gr2	117.70	215.82	0.55	0.21	83%
TB2Gr2	117.70	323.73	0.36	0.23	175%
TB3Gr2	156.60	235.44	0.67	0.26	50%
TB4Gr2	156.96	293.32	0.54	0.30	87%
TB5Gr2	117.70	252.12	0.47	0.23	114%
TB6Gr2	156.60	284.50	0.55	0.29	82%
a/d=1.8					
TB1Gr3	112.80	180.00	0.63	0.19	60%
TB2Gr3	110.00	196.00	0.56	0.21	78%
TB3Gr3	98.00	193.00	0.51	0.20	97%
TB4Gr3	137.00	213.00	0.64	0.22	55%
TB5Gr3	107.90	198.00	0.54	0.22	84%
TB6Gr3	127.50	215.80	0.59	0.22	69%
Average			0.52		
Standard dev.			0.08		

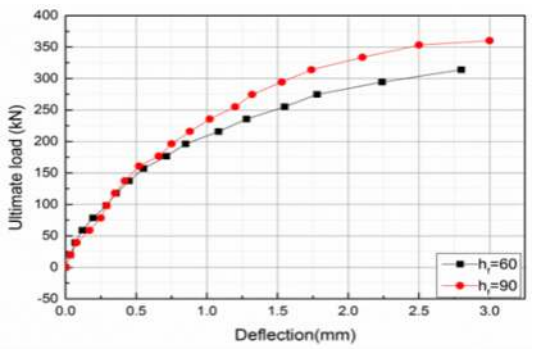

(a) Beams with b_f=360 mm

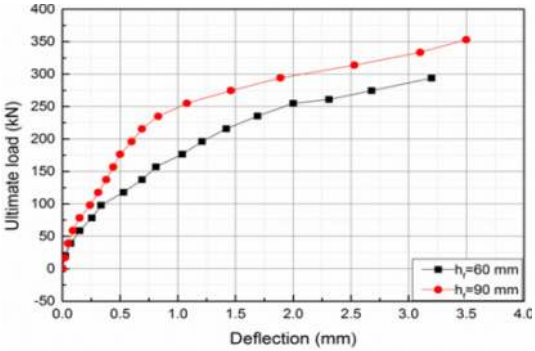

(b) Beams with b_f=300 mm

Fig. 9. Mid span- deflection for tested beams of group 1

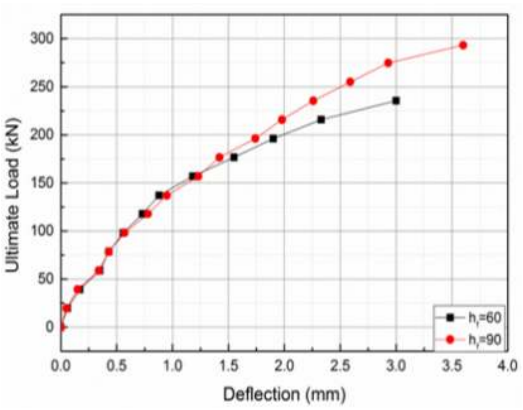

(a) Beams with b_f=360 mm

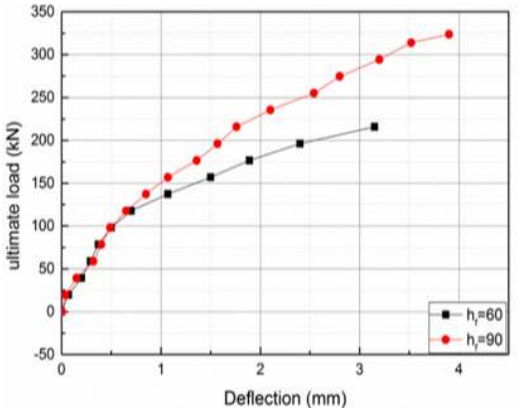

(b) Beams with b_f=300 mm

Fig. 10. Mid span- deflection for tested beams of group 2

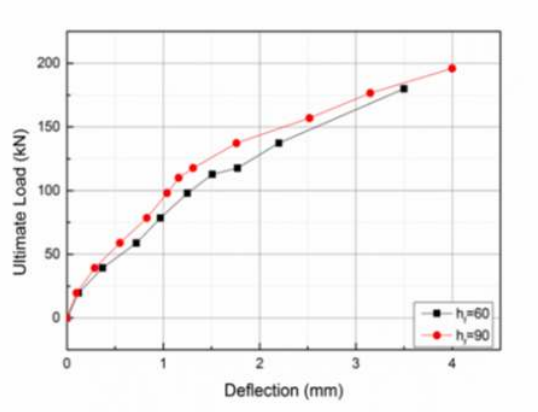

(a) beams with b_f=360 mm

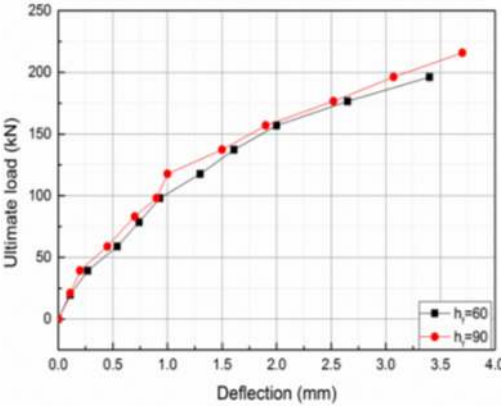

(b) beams with b_f=300 mm

Fig. 11. Mid span-deflection for tested beams of group 3

2.3.10 Concrete strain in the main beam

Fig. 12 represents the typical relationship which illustrates the progression of surface concrete strain with increasing load in three locations of the beams, at mid –span on the mid depth of flange, over the support and on a diagonal line between the upper portion of the center line of the beam and the support plate of the main beams for the eighteen specimens. The measured Longitudinal, vertical, and diagonal concrete strains at points located as shown in Fig. 12. At an early stage of loading the load - strain relationship is linear, but it becomes non-linear at higher loads. Various testing has assigned increasing values in concrete strain associated with first diagonal cracking in testing beams. With different flange width and flange depth under different stress, such as heavily loaded. It's observed that the measured surface strain along the diagonal line between the upper portion of the center line of the beam and the support plate of the main beam is different in beams, because the measured strain were affected by the existence of any crack within the gauge length of the mechanical strain gauge used to measure the strain, therefore, measurements present the concrete strains and crack width.

2.3.11 Inclined crack width

For each load increment, crack width of the major inclined crack propagates at mid-depth of the beam diagonally between load and support is measured by using a hand microscope. Load-crack widths relationships for groups 1, 2 and 3 are shown in Fig. 13 (a, b, and c). It is concluded that: (1) At the same load level, the beams with higher flange depth showed smaller crack width than the beams with smaller flange depth in the same a/d ratio. (2) Flange width exhibits a small effect on crack width. (3) Crack width for tested beams showed a clear tendency to increase with increasing the (a/d) ratio.

3. STM ANALYSIS

3.1 General

The strut- and - tie model (STM) was used by Schlaich et al. [16] as an alternative design procedure. Schlaich et al. [16] distinguish between: B region, where B is referring to Bernoulli concepts; and D region, where D refers to discontinuity. In D region the strain distribution is nonlinear, whereas the distribution in B region is linear. According to the ACI code, D region extends a distance equal to the member depth away from any discontinuity, such as change in cross section (geometric discontinuity) or the presence the constricted loads (static discontinuity). Deep or short beams are a typical example of D region. Generally, The Ultimate Shear strength, Vu, of RC deep beams can be determined by STM. ACI 318 building code [1]; The Canadian standard CSA-A23.3-3-04 [17] and the Euro code [18] induces to use the STM for designing the deep beams with strut and tie method in which the flow of internal forces is modeled; the concrete in uniaxial compression represented by concrete compressive struts, main reinforcement represents the tension ties and nodal zones where the struts and ties meet, are representing the regions of concrete subjected to multidirectional stresses. There is more than one choice of strut and tie model for the same problem in order to transmit the loads through the D regions to support. The two most important factors affecting the type of load transfer mechanism are the shear span-depth ratio (*a*/*d*) of the beams and the amount of transverse reinforcement [19].

3.2 Direct STM

Direct STM means the shear force is carried from the load points toward the supports directly by major compression struts. Fig. 14 shows a typical strut and tie model for two concentration point loads. It can be observed that the model is statically determinate truss containing three components: The concrete strut, the nodal zones and the tie strength of main reinforcing bars. The geometrical notations of the strut-tie method can be shown in Fig. 14.

3.2.1 Top horizontal strut

α_1 is the depth of the horizontal strut as shown in Fig. 14, is defined as a depth of the compression block; can obtain from flexural analysis:

$$a_1 = \frac{A_s f_y}{0.85 f_c` b} \quad (1)$$

Where, f_y and A_S are the yield strength and Area of main steel reinforcement; $f_c`$ is the compressive strength of concrete; and b is the beam width.

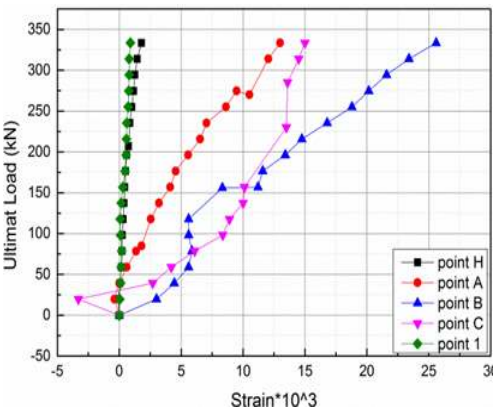

TB1GR1

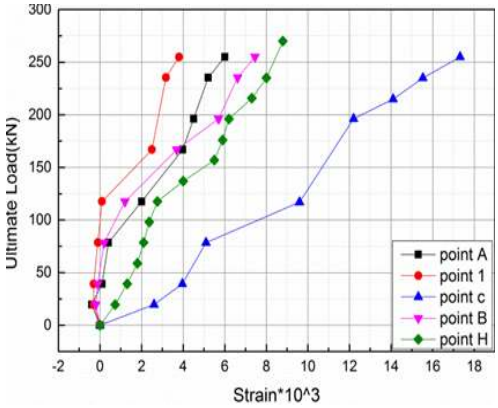

TB2GR1

Fig. 12. Concrete surface strain of tested beams (continued)

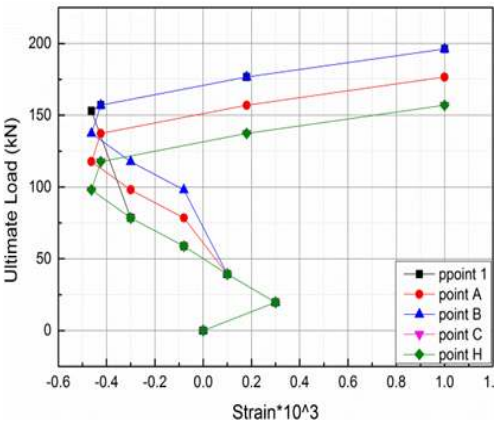

TB1GR2

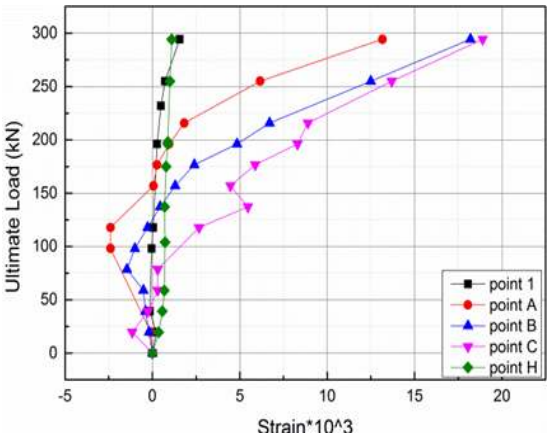

TB2GR2

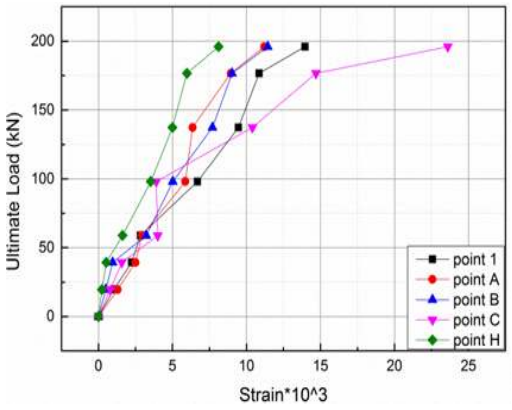

TB5GR3

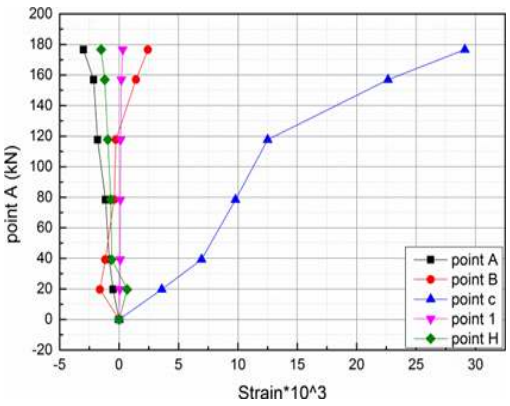

TB6GR3

Fig. 12. Concrete surface strain of tested beams

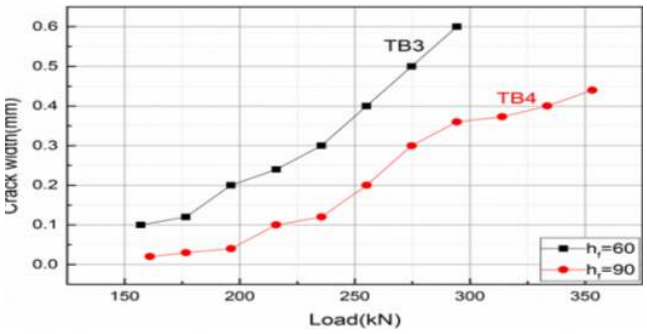

(a) Crack width of beams with b_f= 300 mm of GR1

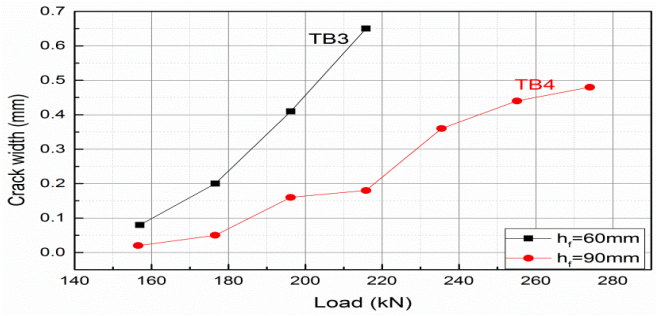

(b) Crack width of beams with b_f= 300 mm of GR2

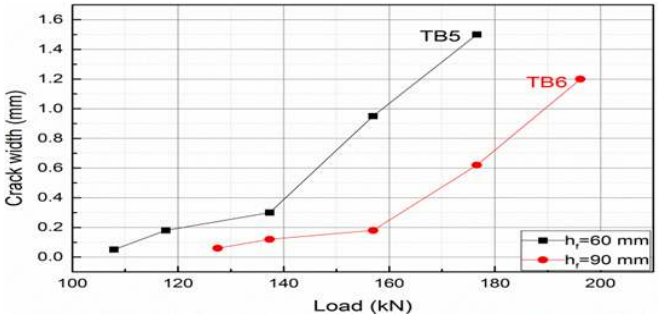

(c) Crack width of beams with b_f= 240 mm of GR3

Fig. 13. Typical crack width of tested beams

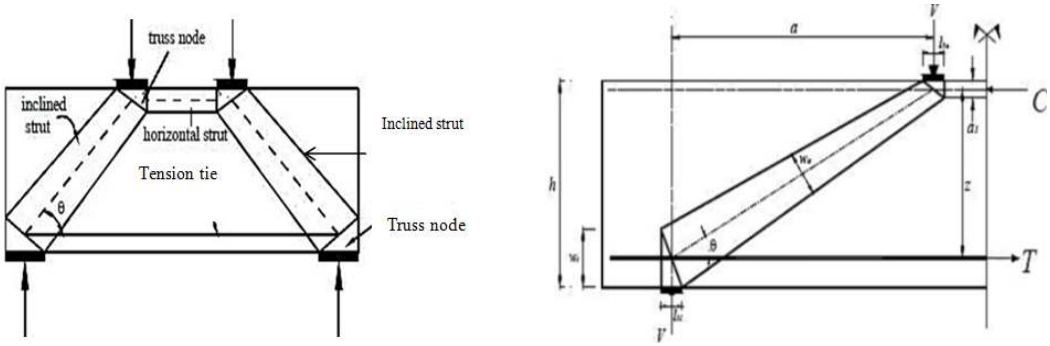

(a) **(b)**

Fig. 14. (a, b)Typical strut-tie model of deep beam

3.2.2 Inclined strut

The upper and lower widths of the inclined strut are determined according to the following equations with respect to Fig. 14.

$$\text{lower width of struct: } w_{st} = l_{bl}\sin\theta + w_t\cos\theta \quad (2)$$

$$\text{upper width of struct: } w_{st} = l_{bu}\sin\theta + a_1\cos\theta \quad (3)$$

Where w_t is the tie width, l_{bl} and l_{bu} are the widths of plates at support and loading point, respectively; and θ is the angle of the inclination strut to the longitudinal axis of the beam and determined as:

$$\theta = \arctan\left(z/a\right) \quad (4)$$

In which

$$z = h - \frac{a_1}{2} - \frac{w_t}{2} \quad (5)$$

In ACI 318-11code the strength of concrete strut F_{ns} is estimated as follows:

$$F_{ns} = f_{ce}A_{cs}$$
$$f_{ce} = 0.85\beta_s f_c' \quad (6)$$

Where f_{ce} is the compressive strength of the concrete in the strut, A_{cs} is the cross–sectional area at one end of the strut, and β_s as recommended by the ACI code. A value of β_s=1 for the top horizontal strut, β_s=0.75 or 0.6 for the inclined strut depending on the existence of web reinforcement.

3.2.3 Reinforcing tie

The effective tie width w_t is usually taken as twice the distance from the extreme tension fiber to the centroid of the main reinforcement of the beam. ACI 318-08 code recommended a practical upper limit of the tie width corresponding to the width in a hydrostatic nodal zone, calculated as:

$$w_{t,\max} = F_{nt}/\left(f_{ce}b\right) \quad (7)$$

Where, F_{nt} is the strength of the tie and f_{ce} is the concrete effective compressive strength in a hydrostatic nodal zone. The strength of the tie, $F_{nt,}$ is calculated as:

$$F_{nt} = A_s f_y \quad (8)$$

Where A_s and f_y are the area and yield strength of tension steel reinforcement.

3.2.4 Nodal zones

The compression strength of a nodal zone, F_{nn}, is calculated such that:

$$F_{nn} = f_{ce}A_{nz}$$
$$f_{ce} = 0.85\beta_n f_c' \quad (9)$$

where A_{nz} is the smallest of: (1) The area of the face of the nodal zone on which the force acts, taken perpendicular to the line of action of the force; (2) The area of a section through the nodal zone, taken perpendicular to the line of the resultant force on the section, f_{ce} is the compressive strength of the concrete in the nodal zone and β_n is the efficiency factor. The Procedure of calculation begins by calculating the compression block's depth α_1, inclination angle θ, area of the strut which is the smaller of the top and bottom nodes, which is used to predict the strut capacity in which the shear force depend on. Furthermore, the tension force in the main steel reinforcement is checkered comparably with force found from the estimated of shear force.

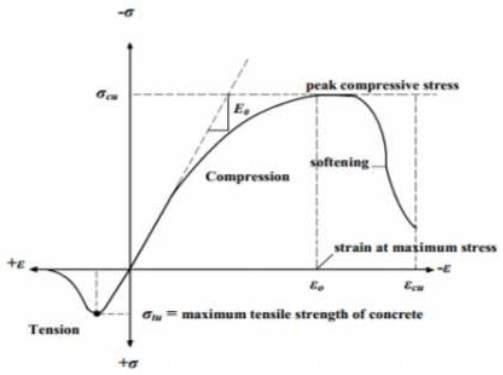

Fig. 15. Stress-strain curve for concrete in

4. FINITE ELEMENT MODEL

FE analysis is done using ANSYS software 12.1 [20]. According to the symmetry of the boundary conditions, materials, and loading, a quarter of the full beam was modeled to reduce the number of element and save much computation time. The model considered to have dimensions, geometry, and configuration with the same as the tested specimens. The element types of the

model are: Structural element SOLID 65 for concrete material to personification non-linearity of brittle material; Element LINK 8 for steel reinforcement; Element SOLID 45 for steel plate in the support and area of applied load. The selected element types are used by Wolanski [21], Kachlakev [22], Mohammed [23] and Hemmaty [24] for material model for analysis the structural stress based on the formulation developed by Williams and Warnke [25]. The transverse shear coefficient is used by Hemmaty [24] in this paper used as (β_t=0.5, β_c=0.95). Fig.15 shows the typical tensile stress-strain and uniaxial compressive relation for concrete [26]. The simplified Uniaxial compressive stress-strain curve for compressed concrete is constructed in this paper by numerical expressions consist Equation 10 used by Desayi [27].

$$f = \frac{E_c \varepsilon}{1+\left(\varepsilon/\varepsilon_0\right)^2} \qquad (10)$$

$$\varepsilon_0 = \frac{2 f_c}{E_c}$$

$$E_c = 4700\sqrt{f}c'$$

Where f the stress at any strain ε, ε is the strain at stress f, and ε_0 is the strain at ultimate compressive strength. Hook's law [28] achieved first point in the curve, which start at $0.30 f_c'$. Points 2, 3, and 4 are finding from Equation 10. Point 5 is at ε_0 and f_c'. Fig. 16 shows the simplified relationship of compressive uniaxial stress-strain used in the stress analysis [29] to help with the convergence of nonlinear solution algorithm. Fig. 17 shows the FE model of one quarter of the beam and mesh. The mesh size used in this paper is (40mm). The Poisson's ratio for concrete and steel used in this study are 0.2and 0.3respectively. Fig. 18 shows the idealized concrete response in tension [30]. The tensile stress–strain which modeled as linear elastic up to a tensile rupture strength off (f_r= $0.62\sqrt{f}c'$) [31]. E_s is 200000MPa. The relation of uniaxial stress-strain for steel reinforcement is idealized as a bilinear curve as elastic-plastic behavior with strain hardening, which is assumed to be identical in terms of both tension and compression as per the European Committee's [32] criterion of von Mises plasticity yielding, as displayed in Fig. 19. The concept of the 3D-failure of concrete surface used by Hawileh [33] is taken into consideration in this study as shown in Fig. 20. Newton-Raphson procedure is taken into account for applying load which is subdivided into increments of series loads that are applied in several steps as shown in Fig. 21.

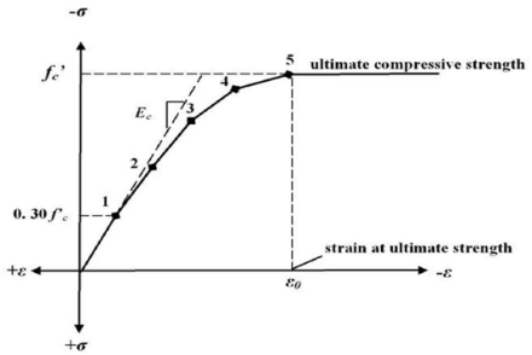

Fig. 16. Simplified Compressive uniaxial stress-strain relationship in concrete

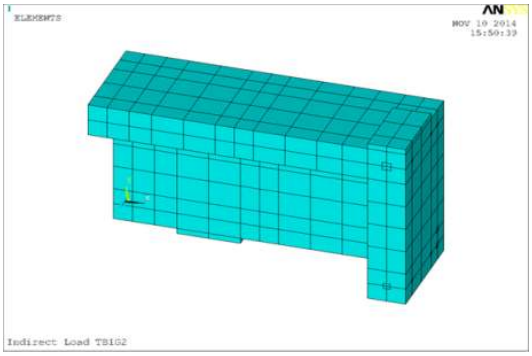

Fig. 17. FE model of one quarter of the beam

5. COMPARISON OF THE EXPERIMENTAL RESULTS WITH THE PREDICTIONS DATA OF STM AND ANSYS MODELS

5.1 Ultimate Shear Capacity

The Ultimate Shear force capacity of test results obtained from 18 deep reinforced concrete T-Beams without web reinforcement are compared with predictions used strut-and-tie model based on ACI code [13] recommendation, as well as to FE Ansys result. Fig. 22 shows that the STM method is very conservative with experimental; the model can be used to estimate the reasonable safer Ultimate Shear force capacity for indirectly loaded deep RC T-beams. Likewise FE results agree with experimental findings. In the otherwise ACI 318-08 building code suggests the theory equation to estimate the shear force of beams loaded by side arms, as below:

$$V_c = \left[0.16\sqrt{f_c'} + 17\rho_w \frac{V_u d}{M_u} \right] b_w d \le 0.29\sqrt{f_c'} b_w d \quad (11)$$

Where $\left(\frac{V_u d}{M_u} \right) \le 1.0$, V_c: Shear strength carried by concrete (kN), M_u: Ultimate bending moment at section consider (kN.m), V_u: Shear strength at ultimate (kN), d: Distance from extreme compression fiber to centroid of tension reinforcement (mm), b_w: Width of beam (mm). The prediction of shear force using equation above is underestimating the shear strength carrying capacity of testing beams.

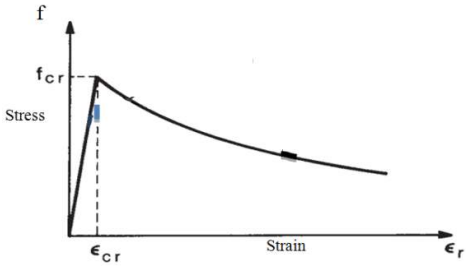

Fig. 18. Stress–strain relationship of concrete in tension

5.2 Mid–span Deflection

Fig. 23 shows the typical experimental and analyzed results estimated by ANSYS with the respect to the mid-span deflection at the centerline of the cross section against the indirect loading. It can be shown that the numerical FE results are close to the experimental data if all factors are well controlled. Curves of FE Ansys load-deflection differ slightly from the experimental curves; this because of, First, existing the micro cracks in the tested concrete specimens which formed through drying shrinkage in the concrete and/or beam handling. On the other hand, the FE models do not deal with micro cracks. Second, the bonding of concrete and steel as perfection in the FE model. However, this supposition is not true for the experimental tests.

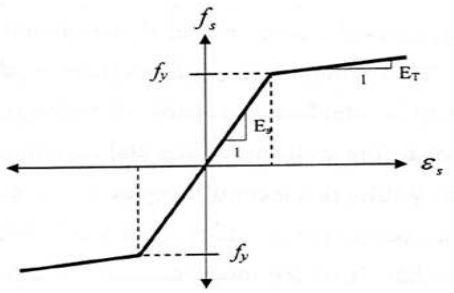

Fig. 19. Modeling of reinforcing bars

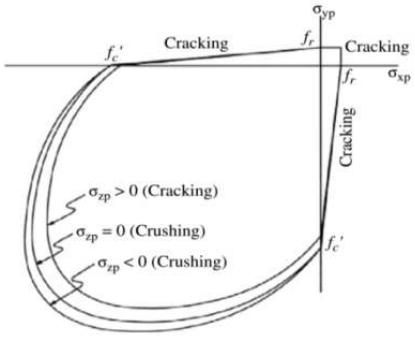

Fig. 20. 3D- failure of concrete surface

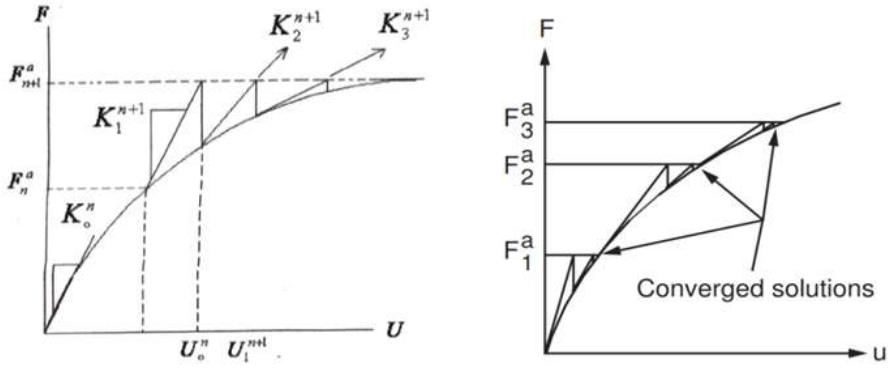

Fig. 21. Full newton-raphson procedure

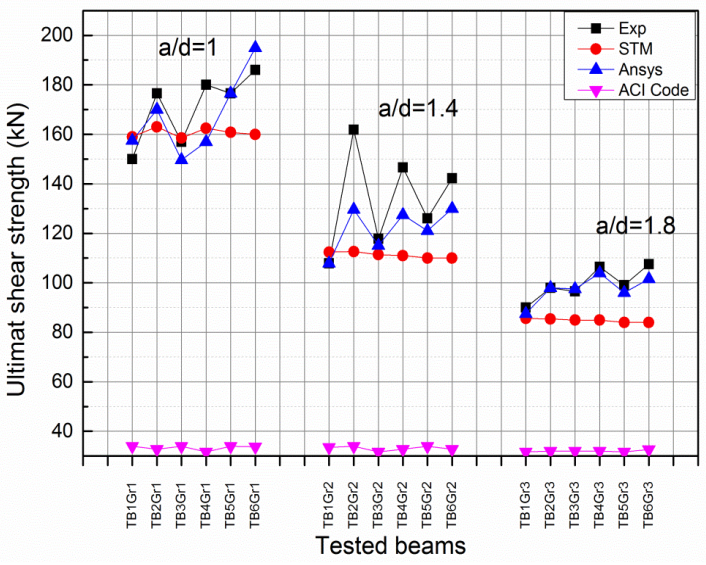

Fig. 22. Ultimate shear strength for tested beams

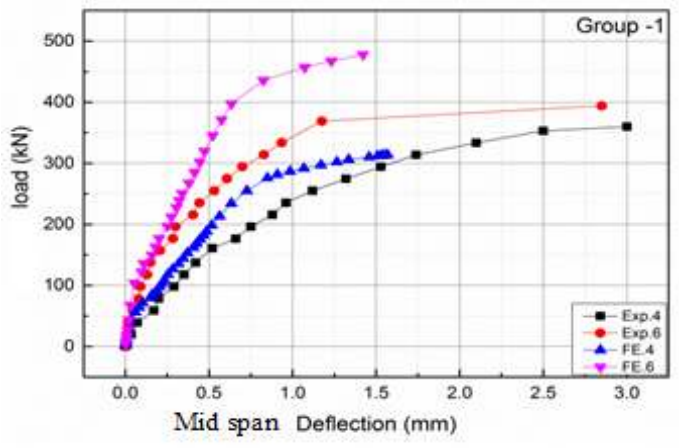

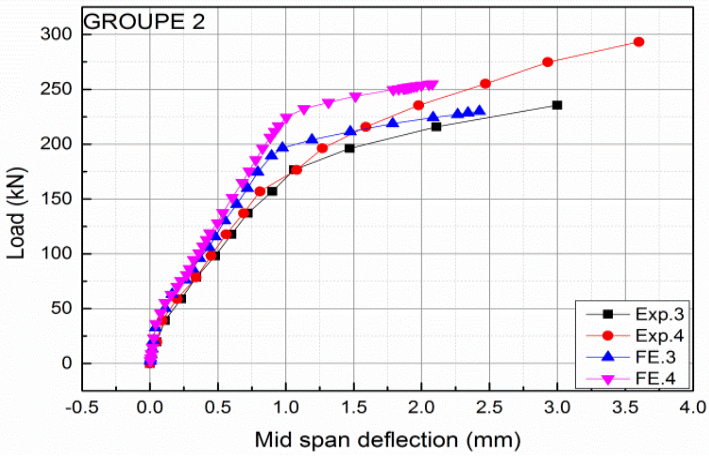

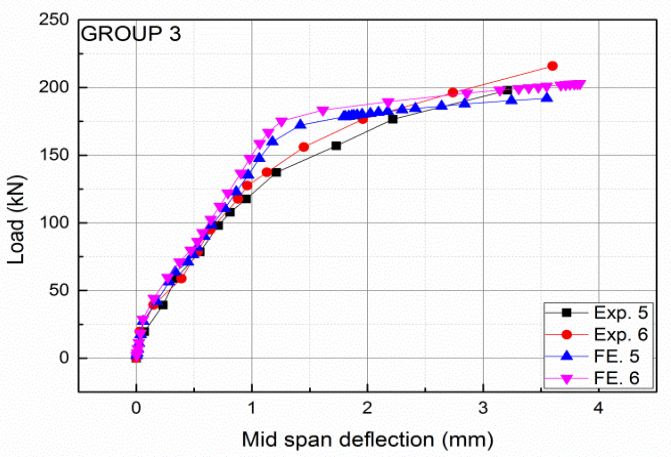

Fig. 23. Experimental and FE ANSYS mid Span Load – Deflection Curves

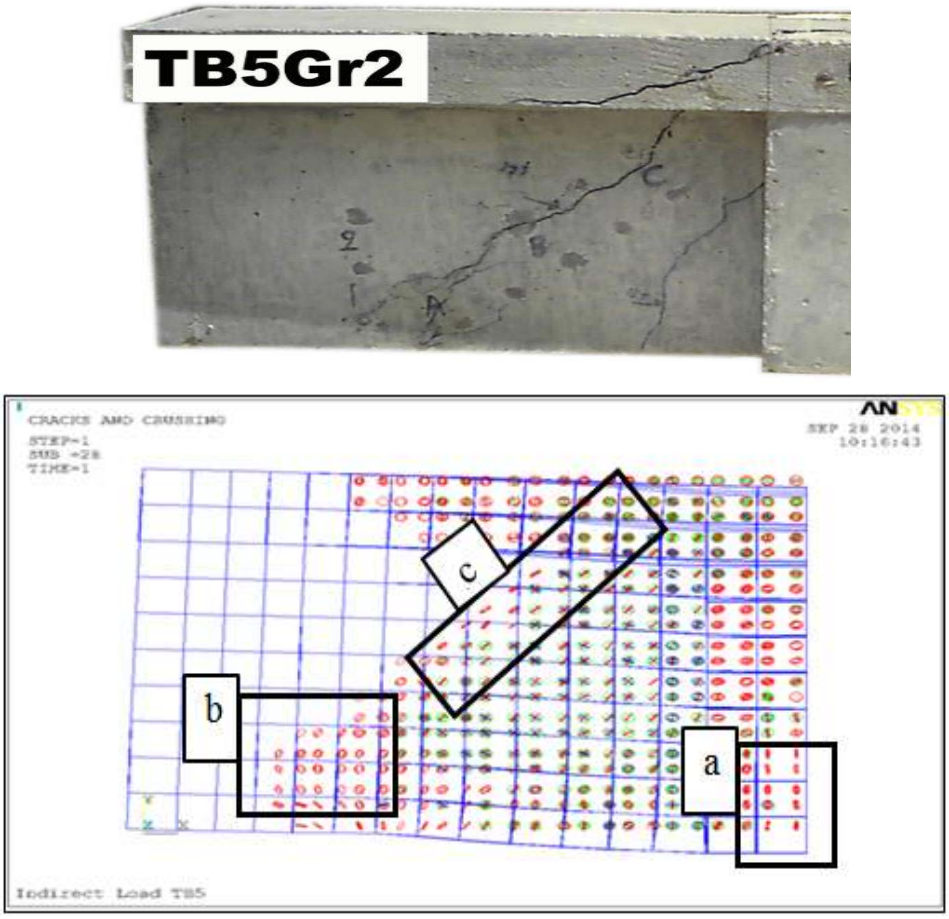

a: flexural cracks, b:compressive cracks, c: diagonal cracks
Fig. 24. Crack patterns at ultimate load appear during experiments and FE analysis

5.3 Crack Patterns

Fig. 24 presents the patterns of cracks appears in ANSYS models for comparison with the tested beams. the study's results confirm the FE analysis and experimental results presented by Özcan et al. [34].

6. CONCLUSION

In this paper, the total of 18 RC Deep T-Beams subjected to indirect points via side arms loading. The general behaviors of beams were examined. The effects of the test parameters such as a/d ratio, flange width and flange depth on the measured Ultimate load capacity of the beams are investigated. The main remarks of the study achieved as the following:

- All the beams fail in shear due to diagonal cracking which leads to the splitting of the beams along the diagonal crack.
- The crack pattern showed that the webs of all beams functioned as simple struts between loads and supports.
- Experimental findings showed that the increasing in flange depth (h_f) of the T-beams in the same (a/d) ratio result in an increased the ultimate load – carrying capacities. From value of non-dimension (R)can be noticed that the beams with the similar flange width and 90 mm flange depth exhibited higher ultimate load than the beams with (h_f) of 60 mm in the same (a/d) ratio. Beams TB2,TB4, and TB6 of group (1) showed 37%, 38%and 10% higher ultimate loads than beams TB1, TB3 and TB5 of group (1); beams TB2, TB4 and TB6 of group (2) showed 10%, 15% and 26% higher ultimate loads than beams TB1, TB3 and TB5 of group (2); beams TB2 and TB4 of group (3) showed 11% and 10% higher ultimate loads than beams TB1 and TB3 of group (3). The same tendency is observed in the case of the respective deflections.
- The mid-span deflection of the indirectly loaded flanged deep beams are small and less than the permissible deflection specified by the ACI Building Code and does not cause any problem at service load (P_u/1.5).
- Both inclined cracking load and ultimate load have a tendency to increase with decreasing the shear span to effective depth ratio below 1.8. An increase of about (50%) in inclined cracking load and (78%) in ultimate load of beam TB5Gr1 and TB5Gr3 is obtained by reducing the (a/d) from 1.8 to 1.
- Inclined crack width is increasing with an increase in (a/d) ratio, as well as it is smaller than for beam with (h_f) of 90 mm than for beam with (h_f) of 60 mm in the same (a/d) ratio.
- The surface concrete strain is linear at early stage of loading but it becomes non-linear at higher loads.
- Mid- span deflection of experimental investigation are closed to those predicted with FE Ansys model.
- The failure mechanism of indirectly loaded deep T-beams is effectively modeled through FE analysis with Ansys model. Moreover, the predicted ultimate failure load with Ansys model has agreed with that obtained during experimental testing.
- STM model is safer for predictions of ultimate strength for member has an arch action mechanism.
- On the other hand the shear strength predicted by using the ACI-318 building Code equation for ordinary beams is under estimating of the shear strength of indirectly loaded deep beams.

COMPETING INTERESTS

Authors have declared that no competing interests exist.

REFERENCES

1. Committee A, Institute AC, Standardization IOf. Building code requirements for structural concrete (ACI 318-08) and Commentary; 2008. American Concrete Institute.
2. Park R, Paulay T. Reinforced concrete structures. Book. 1974;1.
3. Syroka-Korol E, Tejchman J. Experimental investigations of size effect in reinforced concrete beams failing by shear. Engineering Structures. 2014;58:63-78.
4. Tan K, Cheng G. Size effect on shear strength of deep beams: Investigating with strut-and-tie model. Journal of Structural Engineering. 2006;132(5):673-685.
5. Kalyanaraman V, Rayan MA, H-Y Pao. Shear tests of deep beams with flanges. Journal of the Structural Division. 1979; 105(12):2760-2766.
6. Kong FK. Reinforced concrete deep beams; 2006. CRC Press.

7. Fereig S, Smith K. Indirect loading on beams with short shear spans. in ACI Journal Proceedings; 1977. ACI.
8. Heywood R, Pritchard R, Shaw P. Assessment of bridges–challenging the structural engineering profession.
9. Ferguson PM. Some implications of recent diagonal tension tests. In ACI Journal Proceedings; 1956. ACI.
10. Taylor R, Some shear tests on reinforced concrete beams without shear reinforcement*. Magazine of Concrete Research. 1960;12(36):145-154.
11. Taub J, Neville A. Resistance to shear of reinforced concrete beams. in ACI Journal Proceedings; 1960. ACI.
12. Zsutty T. Shear strength prediction for separate catagories of simple beam tests. In ACI Journal Proceedings; 1971. ACI.
13. Standard AA. Building code requirements for structural concrete (ACI 318-11); 2011.
14. C39 A. Standard Test Method for Compressive Strength of Cylindrical Concrete Specimens; 2010.
15. 426, A.-A.C. The Shear Strength of Reinforced Concrete Members. in ACI Journal Proceedings; 1973. ACI.
16. Schlaich J, et al. Toward a consistent design of structural concrete. PCI Journal. 1987;(32).
17. Standard C. A23. 3-04. Design of concrete structures, Canadian Standard Association; 2004.
18. Institution BS. Eurocode 2: Design of concrete structures: Part 1-1: General Rules and Rules for Buildings; 2004. British Standards Institution.
19. Brena SF, Roy NC. Evaluation of load transfer and strut strength of deep beams with short longitudinal bar anchorages. ACI Structural Journal. 2009;106(5).
20. ANSYS C. Help Manual 12.1.
21. Wolanski AJ. Flexural behavior of reinforced and prestressed concrete beams using finite element analysis; 2004. Citeseer.
22. Kachlakev D, et al. Finite element Modeling of concrete structures strengthened with FRP laminates. Final report, SPR. 2001;316.
23. Ibrahim AM, Mahmood MS. Finite element modeling of reinforced concrete beams strengthened with FRP laminates. European Journal of Scientific Research. 2009;30(4):526-541.
24. Hemmaty Y. Modeling of the shear force transferred between cracks in reinforced and fiber reinforced concrete structures. In Proceedings of the ANSYS Conference; 1998.
25. Willam K, Warnke E. Constitutive model for the triaxial behavior of concrete. In Proceedings, International Association for Bridge and Structural Engineering. ISMES, Bergamo, Italy; 1975.
26. Bangash M. Concrete and concrete structures: Numerical Modelling and Applications; 1989.
27. Desayi P, Krishnan S. Equation for the stress-strain curve of concrete. in ACI Journal Proceedings; 1964. ACI.
28. Gere JM, Timoshenko SP. Mechanics of materials. PWS, Boston; 1997.
29. Fanning P. Nonlinear models of reinforced and post-tensioned concrete beams. Electronic Journal of Structural Engineering. 2001;1:111-119.
30. Vecchio F, Collins M. Stress-strain characteristics of reinforced concrete in pure shear. Final Report. 1981;211-225.
31. Standard AA. Building code requirements for structural concrete (ACI 318-14); 2014.
32. Certificación Y, A.E.d.N. Eurocode 3: Design of steel structures–Part 1-1: General rules and rules for buildings. UNE-EN. 1993;1-1.
33. Hawileh R, et al. Modeling of insulated CFRP-strengthened reinforced concrete T-beam exposed to fire. Engineering Structures. 2009;31(12):3072-3079.
34. Özcan DM. et al. Experimental and finite element analysis on the steel fiber-reinforced concrete (SFRC) beams ultimate behavior. Construction and Building Materials. 2009;23(2):1064-1077.

Peer-review history:
The peer review history for this paper can be accessed here:
http://sciencedomain.org/review-history/14277